DR M. P. ALBANO (Orcid ID : 0000-0002-5235-0032)

Article type : Article

COLLOIDAL PROCESSING OF Al_2O_3-DOPED ZIRCONIA CERAMICS WITH CaO-P_2O_5-SiO_2 GLASS AS ADDITIVE

Clara G. Soubelet[a], María P. Albano[a]

[a]Centro de Tecnología de Recursos Minerales y Cerámica (CETMIC), C.C . 49 (B1897ZCA) M. B. Gonnet, Provincia de Buenos Aires, ARGENTINA. Fax 54 (0221) 471-0075.E-mail:palbano@cetmic.unlp.edu.ar

ABSTRACT

Well dispersed concentrated aqueous suspensions of Al_2O_3-doped Y-TZP (AY-TZP), AY-TZP with 5.4 vol% of CaO-P_2O_5-SiO_2 (CaPSi) glass (AY-TZP5) and 10.5 vol% CaPSi glass (AY-TZP10), with ammonium polyacrylate (NH_4PA) dispersant were prepared to produce slip cast compacts. The rheological properties of 35 and 40 vol% slips were studied. The densification, microstructure as well as hardness and fracture toughness were investigated as a function of CaPSi glass content at 1300-1500 ºC. The optimum NH_4PA concentration of 35 vol% AY-TZP5 and AY-TZP10 slips at pH ~9 was found to be about 43 and 67 % greater than that of AY-TZP slips, this behaviour was related to the greater amounts of Ca^{2+} ions leached out from the CaPSi glass surface. The viscosity of stabilized 40 vol% slips with NH_4PA attained a minimum value at 5.4 vol% CaPSi glass addition, and resulted in a more dense packing of cast samples. AY-TZP5 can be sintered at a lower temperature (1300 ºC) compared to that of AY-TZP. AY-TZP5 exhibited a fine microstructure of tetragonal ZrO_2 (grain sizes below 0.3 μm), and

This article has been accepted for publication and undergone full peer review but has not been through the copyediting, typesetting, pagination and proofreading process, which may lead to differences between this version and the Version of Record. Please cite this article as doi: 10.1111/IJAC.13420

$ZrSiO_4$ - $Ca_2P_2O_7$ particles homogeneously distributed within the zirconia matrix. Its presented similar fracture toughness and a slightly lower hardness compared to those of AY-TZP.

Keywords: Al_2O_3-doped zirconia with CaO-P_2O_5-SiO_2 glass additive, rheological properties, slip casting, sintering behaviour, microstructure.

1. INTRODUCTION

3 mol% partially stabilized zirconia (Y-TZP) ceramics are frequently used as dental restorations and dental implant materials due to their attractive properties, including high flexural strength and fracture toughness, inertness in biological fluids, good biocompatibility and aesthetics[1-3].

It has been well documented[4,5] that the addition of glasses enhanced the Y-TZP densification. We have recently demonstrated[6] that the addition of a sol-gel derived CaO-P_2O_5-SiO_2 (CaPSi) glass produced low amounts of $Ca_2P_2O_7$ which improved the osteoblast cell response of sintered Y-TZP ceramics. Apart from the biological properties, another aspect to be considered in Y-TZP ceramics is the hydrothermal degradation or ageing which results in the drop of mechanical properties. It is generally accepted[7-9] that the tetragonal (t) to monoclinic (m) zirconia (ZrO_2) transformation induced by hydrothermal treatment is strongly dependent on its grain size, this transformation would be inhibited in a fine zirconia grain microstructure. Besides, some studies[10,11] have shown that the Al_2O_3 -doping had a positive effect on the ageing resistance of Y-TZP ceramics. Wu et al[11] reported that the introduction of 0.5-5 wt% Al_2O_3 into Y-TZP effectively delayed the t-m ZrO_2 transformation and the degradation of mechanical properties. In this work, an Al_2O_3-doped Y-TZP powder referred as AY-TZP, with higher sinterability compared to that of undoped-Y-TZP powder was used. It is expected that the addition of CaPSi glass to AY-TZP will reduce its sintering temperature; in this way a fine ZrO_2 grain microstructure could be obtained. In addition, the additional phases produced during CaPSi glass thermal treatment could have a positive effect on the ageing behaviour by decreasing the m-ZrO_2 surface content and retarding the propagation of the t-m ZrO_2 transformation. The combined effects of the Al_2O_3-doping, the fine ZrO_2 grains, and the

present of additional phases, are expected to improve the ageing resistance increasing the reliability of dental restorations based on zirconia.

Colloidal shaping methods such as slip casting enable to achieve green compacts with high microstructural homogeneity[12-14]. Repulsive interactions between particles can be generated by the addition of polyelectrolytic additives[15-17]. In the present work, ammonium polyacrylate (NH_4PA) was used as dispersant of AY-TZP and AY-TZP-CaPSi glass powders in aqueous media. The adsorption of the polyelectrolyte at the particle surface infer repulsive particle forces caused by electrostatic and steric effects. The magnitude of the inter particle forces are closely related to the net surface charge density of the NH_4PA adsorbed-powder, and the conformation of the polyelectrolyte in solution. The CaO-P_2O_5-SiO_2 glasses are known[18,19] to leach Ca^{2+} ions by a Ca^{2+} /H^+ exchange reaction at the glass-solution interface. Ca^{2+} leached out from the glass surface during the aqueous processing of AY-TZP-CaPSi suspensions with NH_4PA could result in increased NH_4PA adsorption, affecting the colloidal stability of concentrated slips. The control of both the state of the dispersion and the rheological properties are of great importance to perform a successful colloidal processing of AY-TZP-CaPSi ceramics. Stabilized suspensions will produce sintered compacts with high densities and homogeneous microstructures.

In this work, the influence of CaPSi glass addition on the colloidal stability and rheological properties of 35 and 40 vol% AY-TZP slips was studied. The characterization of the different suspensions was completed with a time-dependent viscosity study. In addition, the densification behaviour, microstructure as well as hardness and fracture toughness were investigated as a function of CaPSi glass content and sintering temperature.

2. EXPERIMENTAL PROCEDURE

2.1. Raw materials and powder processing

The starting powder was a commercial 3 mol% yttria- partially stabilized zirconia with 0.25 wt% Al_2O_3 (AY-TZP) (Saint-Gobain ZirPro, China). The synthesis of the CaO-P_2O_5-SiO_2 glass with composition: 26% CaO, 10% P_2O_5 and 64% SiO_2 (based on mol%),named CaPSi in this work, was performed by the sol-gel method; details of the experimental procedure are given elsewhere[20]. Milling of the glass powder was done by

attrition milling in isopropyl alcohol using 1.6 mm zirconia balls during 4 h, then the powder was dried at 60 ^{o}C for 24 h. The measured density of the CaPSi glass was 2.70 g/cm^3.

Al_2O_3-doped Y-TZP (AY-TZP), AY-TZP with 5.4 vol% CaPSi glass (AY-TZP5), and AY-TZP with 10.5 vol% CaPSi glass (AY-TZP10) ceramics were investigated in this study. A commercial ammonium polyacrylate (NH_4PA) solution (Duramax D 3500, Rohm & Haas, Philadelphia PA) was used as dispersant. 35 vol% aqueous AY-TZP and AY-TZP-CaPSi suspensions with the different compositions and various amounts of dispersant were prepared by dispersing particles in deionized water using an ultrasonic bath. The pH was manually adjusted at 9 with a diluted aqueous ammonia solution only for AY-TZP suspensions. For AY-TZP-CaPSi slips the pH rose spontaneously to ~9 (see section 3.2).

In order to study the influence of the solid loading on the rheological properties, slips with the optimum NH_4PA concentration and a solid content of 40 vol% were prepared at pH ~9. 40 vol% slips were cast in plaster molds into 1.85 cm diameter disks. The consolidated disks were air dried at room temperature followed by 24 h at 100 ^{0}C. The resulting green compacts were sintered in air at 1300-1500 ^{0}C during 2h with a heating/cooling rate of 10 ^{0}C/min.

2.2. Characterization techniques

The particle size distributions of AY-TZP and CaPSi glass powders were measured using a Mastersizer 2000 (Malvern Instruments, UK).

To determine the isoelectric point (IEP) of the powders, zeta potential against pH curves were measured with an instrument Zetasizer nano ZS (Malvern Instruments, UK) for 0.05 vol% AY-TZP and CaPSi glass suspensions in the pH range of 2-12. Zeta potential versus pH curves were also measured for 0.05 vol% slips of AY-TZP and AY-TZP-CaPSi with the optimum amount of NH_4PA at pH 1-12. The pH adjustment was achieved with HCl or NH_4OH solutions. The pH was measured with a pH meter calibrated with buffer solutions (pH 4, 7 and 10, Merck, Germany). Each curve was repeated three times.

Steady state flow curves of the different suspensions were performed using a concentric cylinder viscometer (Haake VT550, Germany) at 25 °C. A coaxial cylinder

system with two gaps (sensor system NV Haake) was used. The steady shear stress value was measured as a function of shear rate in the 0.5 - 542 s^{-1} shear rates range. As soon as stationary conditions were reached at each shear rate, the shear rate increased in steps up to the maximum value and then decreased. The thixotropic behaviour was investigated by evaluating the hysteresis loop areas obtained through the flow curves of shear stress versus shear rate. The hysteresis loop area was the area enclosed by the up and down curves, and it was calculated as the difference between the areas under the up and down curves.

The density of the green compacts was determined by the Archimedes method using mercury displacement. The Archimedes method with distilled water as the immersion liquid was employed to determine the bulk density of the sintered compacts; a theoretical density of 6.05 g/cm^3 was used to calculate the relative density of AY-TZP. The theoretical density of the sintered AY-TZP5 and AY-TZP10 compacts at each temperature was calculated from the density values of the different phases and their respective volume fraction.

Crystalline phases were characterized by X-ray diffraction (Bruker, D2 Phaser, with Kα: Cu as incident radiation and Ni filter); the equipment was operated at 30 kV and 10 mA and the scanning was performed with a step of 0.04° and 2.5 s per step in the 10°-80° 2θ range. In order to perform phase quantification, the XRD patterns were analysed with PROGRAM FullProf.2k (Version 5.80 - May 2016-ILL JRC) which is a multipurpose profile-fitting program, including Rietveld refinement method[21,22]. The morphology of the phases was observed by scanning electron microscopy (SEM) (FEI, Quanta 200); compositional analysis was performed by energy dispersive x-ray spectrometry (EDS).

The sintered samples were diamond polished down to 3 μm and thermally etched at a temperature 50 ^{0}C below each sintering temperature for 30 min. The zirconia (ZrO_2) grain sizes of the sintered compacts were measured from SEM images using Image J software according to the linear interception method.

The Vickers hardness (Hv) was measured using a diamond indenter (Buehler hardness tester) with a holding time of 15 s under a load of 3 Kgf. Hv was calculated by:

$$Hv = 1.854\ (F/d^2) \qquad (1)$$

Where d is the arithmetic mean of two diagonals (d_1 and d_2) and F is the indentation load. The reported Hv values are the mean ± standard deviation of ten identations. The crack propagation path after Vickers indentation was observed by SEM.

The fracture toughness (K_{1c}) was calculated on the basis of the indentation method by the equation:

$$K_{1c}=0.016\ (E/H)^{1/2}\ (P/C^{3/2}) \qquad (2)$$

Where C is the crack length measured using the ocular on the hardness tester, P the indentation load, E is the Young's modulus and H the vickers hardness.

3. RESULTS

3.1. Powder characterization

Figure 1 shows the particle size distribution curves of AY-TZP and CaPSi glass powders. The AY-TZP powder exhibited an unimodal distribution with a more frequent particle diameter of 0.14 μm. Particle sizes between 1 and 13 μm, and a more frequent particle diameter of 3 μm were found for the CaPSi glass.

Figure 2 shows the zeta potential versus pH curves of AY-TZP and CaPSi glass powders. The IEP of AY-TZP powder was found to be about 6.5, indicating that the surface charge of AY-TZP was negative at pH > 6.5. On the contrary, CaPSi glass powder had a negative surface charge in the whole pH range studied; and a slightly increase in the negative surface charge with increasing pH was found. Similar negative zeta potential values at pH 9, -26 mV for CaPSi and -29 mV for AY-TZP, were measured for both powders.

3.2. Colloidal stability and rheological properties

Figures 3a, 3b and 3c show the flow curves of viscosity versus shear rate as a function of the amount of NH_4PA solution added at pH ~9 for 35 vol% AY-TZP, AY-TZP5 and AY-TZP10 slips, respectively. For the different compositions the viscosity values decreased with increasing shear rate, thus the suspensions exhibited a shear thinning behaviour. The measured flow curves of shear stress versus shear rate were satisfactorily fitted with the power-law model over the whole range of shear rates tested. The power-law model equation can be expressed as:

$$\tau = k\ \gamma^n \qquad (3)$$

Where τ is the shear stress (Pa), γ is the shear rate (s^{-1}), k is called the consistency index ($Pa.s^n$) and n is the flow behaviour index (dimensionless). The k constant is proportional to the viscosity and the n constant, which is < 1for shear thinning behaviour, indicates the degree of shear thinning. The effect of NH_4PA concentration on the power-law model fitting parameters, k and n, of the up flow curves for 35 vol% AY-TZP, AY-TZP5 and AY-TZP10 slips, is shown in table 1. All the analysed slips presented correlation coefficient (R^2) values in the range of 0.98-1.0, indicating a good correlation to the power-law model.

The AY-TZP slips with 0.51 wt% NH_4PA was weakly flocculated with higher viscosity values throughout the whole shear rate range (fig. 3a); as a consequence a higher k value was measured for this flocculated suspension (table 1). Further additions of polymer resulted in a decrease in k, for 0.88 wt% NH_4PA the viscosity and consequently k attained the minimum values (figs. 3a and table 1). The AY-TZP suspensions changed from being weakly flocculated for 0.51 wt% NH_4PA to well stabilized for 0.88 wt% NH_4PA addition.

At pH 9 the anionic polyelectrolyte is fully dissociated. The zeta potential versus pH curves of AY-TZP with 0.88 wt% NH_4PA (optimum NH_4PA concentration) showed that the adsorption of the polyelectrolyte shifted the pH_{IEP} of AY-TZP from 6.5 (fig. 2) to 3.1 (fig. 4), and resulted in an increasingly negative surface charge at a given pH. The magnitude of the negative zeta potential of the AY-TZP powder at pH 9 increased from -29 mV for 0 wt% NH_4PA to -47 mV for 0.88 wt% NH_4PA. The adsorption of the negatively charged polyelectrolyte induces electrostatic and steric forces between particles[23]. The magnitude of the inter particle repulsive forces at pH 9 was related to the amount of NH_4PA adsorbed. For 0.51 wt% NH_4PA, the incomplete adsorption of the polyelectrolyte produced lower electrostatic repulsion between particles, forcing particles together and promoting their flocculation. The aggregated particles increased the resistance to flow and immobilized some of the liquid available for flow, leading to high viscosity values. For 0.88 wt% NH_4PA the suspension was dominated by electrosteric repulsive forces, greater NH_4PA addition (1.02) increased the viscosity due to an excess of polymer in solution. For AY-TZP slips, the constant n was in the range 0.31-0.36, reaching the maximum value for 0.88 wt% NH_4PA.

For AY-TZP5 slips with 1.07 wt% NH_4PA (figs. 3b and table 1), the high viscosity and k values indicated a strong flocculation, and the low n value suggested a strong

shear thinning behaviour. The addition of greater amounts of NH_4PA produced a reduction in the viscosity and k values and an increase in n. The optimum state of dispersion for 35 vol% AY-TZP5 slips was achieved by the addition of 1.26 wt% NH_4PA. The degree of shear thinning had a maximum value for 1.26 wt% NH_4PA.

The rheological behaviour of AY-TZP10 (figs. 3c and table 1) showed that a greater amount of NH_4PA (1.47 wt%) was necessary to attain a stabilized suspension. For 1.47 wt% NH_4PA, minimum viscosity and consequently k values were found. It can be noticed the reduction in the degree of shear thinning at the optimum state of dispersion for all the slip compositions (table 1).

Figure 5 shows the variation of pH with increasing solid concentration during the aqueous colloidal processing of 35 vol% AY-TZP, AY-TZP5 and AY-TZP10 suspensions. The addition of 1.19 g/ml of AY-TZP to the aqueous solution produced an increase in pH from 7.25 to 8.38, whereas a greater increase in pH to 8.90 and 9.32 was observed by the addition of 0.72 g/ml of AY-TZP5 and 0.76 g/ml of AY-TZP10. The pH remained nearly constant with increasing the solid concentration over 1.19 and 0.72-0.76 g/ml of AY-TZP and AY-TZP5-AY-TZP10, respectively.

For all the suspensions, the measured shear stress and hence the viscosity decreased with time under the constant shear. A decrease of the viscosity under shear stress due to the progressive break down of the structure, followed by a gradual recovery of the structure when the stress is removed is called “thixotropy”. Thus, thixotropy is the property exhibited by shear thinning suspensions which show time-dependent change in the viscosity[24]. The area enclosed by the up and down flow curves of shear stress against shear rate, is referred to as hysteresis loop[24,25]. It is generally admitted that the area of hysteresis loops can be considered as an estimation of the degree of thixotropy; the greater the hysteresis area is the stronger are the thixotropic properties. The hysteresis loop area as a function of the NH_4PA concentration for the different 35 vol% slips, is presented in Figure 6. A strong thixotropic behaviour was observed for flocculated slips: AY-TZP with 0.51 wt% NH_4PA, AY-TZP5 with 1.07 and 1.16 wt% NH_4PA and AY-TZP10 with 1.18 wt% NH_4PA (figs. 3). Whereas the minimum hysteresis loop area was found at the optimum NH_4PA concentration for each slip composition.

Figures 7a and 7b show the viscosity versus shear rate curves for 35 and 40 vol% stabilized slips, respectively, at pH ~9. The effect of CaPSi glass content on the k

rheological parameter of the up flow curves, is presented in Figure 8 for the different solid loading. Well dispersed 35 vol% slips with low viscosities and k values were obtained; the viscosity and k values of the slips with different CaPSi glass additions were similar (figs. 7a and 8). The n parameter scarcely changed from 0.36 for AY-TZP to 0.34 for AY-TZP5-AY-TZP10. Thus, the rheological behaviour of stabilized 35 vol% slips did not significantly change by the addition of CaPSi glass. A different behaviour was found for 40 vol% slips; minimum viscosity and k values were found at 5.4 vol% CaPSi glass (figs. 7b and 8). A similar shear thinning tendency was observed for AY-TZP (n=0.36) and AY-TZP5 (n=0.36) with respect to AY-TZP10 (n=0.34) slips.

The hysteresis loop area as a function of the CaPSi glass content for stabilized slips with different volume fraction of solids, is shown in figure 9. For 35 vol% slips, the hysteresis area remained nearly constant with increasing CaPSi glass content from 0 to 5.4 vol%, over 5.4 vol% CaPSi the hysteresis area decreased. On the contrary, for 40 vol% slips the hysteresis area was reduced by the addition of 5.4 vol% CaPSi glass.

3.3. Sintering and characterization of sintered samples

The green density of cast samples prepared from stabilized 40 vol% AY-TZP, AY-TZP5 and AY-TZP10 slips was 58.4, 60.4 and 55.0% of theoretical density, respectively. Thus, the addition of 5.4 vol% CaPSi glass decreased the slip viscosity with NH_4PA (figs. 7b and 8), and resulted in a more dense packing of cast samples.

Table 2 presents the relative density and mechanical properties of the different samples sintered at 1300-1500 ^oC. The relative density of AY-TZP increased with increasing sintering temperature from 1300 to 1400 ^oC, reaching ~99% of the theoretical density (T.D.) at 1400 ^oC. AY-TZP5 attained nearly full densification at a lower temperature (1300 ^oC) with respect to that of AY-TZP. At 1500 ^oC a decrease in the sintered density of AY-TZP and AY-TZP5 was found, this behaviour will be explained in section 4. The relative density of AY-TZP10 was lower than 96% T.D. at 1300-1400 ^oC and reached ~96% T.D. at 1500 ^oC. A SEM image of AY-TZP10 at 1300 ^oC (figure 10a) showed some large pores, indicating that the elimination of porosity was not completed. On the contrary, AY-TZP5 fully dense at 1300 ^oC can be observed in figure 10b. The lower sintered densities of AY-TZP10 in the temperature range examined could be attributed to their lower green packing density.

The crystalline phase contents of the samples sintered at 1300-1500 °C are shown in table 3. Only the tetragonal ZrO_2 phase was present in AY-TZP at 1300-1400 °C. In AY-TZP5 and AY-TZP10 at 1300-1400 °C, the major crystalline phase was t- ZrO_2 accompanied by minor amounts of additional phases ($ZrSiO_4$ and $Ca_2P_2O_7$). A SEM image of AY-TZP5 at 1400 °C (figure 10c) show polygonal particles of $ZrSiO_4$ and elongated ones of $Ca_2P_2O_7$, distributed in the tetragonal ZrO_2 fine grain matrix. The thermal decomposition of the CaPSi glass at 950-1500 °C produced SiO_2 as a major phase and calcium phosphate as a minor one[6]. A reaction occurred between ZrO_2 and most of the SiO_2 produced by CaPSi glass annealing, leading to the formation of $ZrSiO_4$[6]. The total content of additional phases ($ZrSiO_4$ + $Ca_2P_2O_7$) increased with increasing the CaPSi glass content from ~4.5 vol% for AY-TZP5 to ~8.4 vol% for AY-TZP10, irrespective of the sintering temperature.

At 1500 °C, a small amount of m- ZrO_2 appeared in AY-TZP and the addition of CaPSi glass markedly promoted the t-m transformation (table 3). It is generally admitted[7], that larger ZrO_2 grains enhance the spontaneous t-m transformation after sintering. In order to clarify the effect of the sintering temperature and CaPSi glass content on the stability of t- ZrO_2, the ZrO_2 grain size distributions of the different samples at 1300-1500 °C are plotted in figure 11. The more frequent grain size of AY-TZP increased from 0.17 μm at 1300 °C to 0.55 μm at 1500 °C, thus the AY-TZP curves were shifted to greater sizes with increasing temperature. AY-TZP at 1300 °C and 1400 °C exhibited narrow distributions, having grain sizes in the range 0.07-0.25 μm at 1300 °C and 0.25-0.50 μm at 1400 °C; a wider grain size distribution with grain sizes between 0.30 and 0.85 μm was found at 1500 °C. Thus, the wide of the ZrO_2 grain size distribution increased gradually up to 1400 °C and then rapidly above this temperature.

The XRD patterns of AY-TZP at 1300-1500 °C in the 2θ range of 26.5-27.7° are shown in figure 12. In this 2θ range, reflection peaks of t- ZrO_2 and m- ZrO_2 are not present, and peaks corresponding to the segregation of different phases at grain boundaries can be distinguished. XRD patterns of AY-TZP at 1300-1400 °C revealed the presence of $Y_2Hf_7O_{17}$ traces; the formation of this phase can be attributed to the segregation of Y^{3+} and Hf^{4+} ions, included in the starting AY-TZP powder to grain boundaries. This result suggested that dominantly Y^{3+} along with Hf^{4+} ions migrated in the

direction of grain boundaries at 1300-1400 ^{o}C. It should be pointed out that an yttria content of 2.3-2.5 mol% (estimated by EDS analysis) in the AY-TZP grains, which corresponded to that of the tetragonal phase, was measured at 1300-1500 ^{o}C. On the contrary at 1500 ^{o}C, a high well-defined XRD peak of Al_3Hf appeared. Clearly, the Al^{3+} ions segregation to grain boundaries was enhanced at 1500 ^{o}C; thus, Al^{3+} ions rather than Y^{3+} ions segregated at grain boundaries at 1500 ^{o}C.

An interesting result of this work was related to the effect of the CaPSi glass addition on the ZrO_2 grain size distribution of AY-TZP, at each sintering temperature (fig. 11). At 1300-1400 ^{o}C, the addition of glass scarcely shifted the ZrO_2 grain size distribution of AY-TZP to greater sizes; the more frequent grain size of AY-TZP5 and AY-TZP10 were close to that measured for AY-TZP. AY-TZP5- AY-TZP10 at 1300 ^{o}C and 1400 ^{o}C exhibited a greater volume of grains above 0.24 and 0.46 μm, respectively, compared to those of AY-TZP. On the contrary, the ZrO_2 grain size distribution of AY-TZP at 1500 ^{o}C was markedly shifted to greater sizes by the addition of CaPSi glass; the more frequent grain size increased from 0.55 μm for AY-TZP to 0.70 and 0.75 μm for AY-TZP5 and AY-TZP10, respectively. A lesser volume of grains between 0.30 and 0.68 μm and a greater volume of grains in the range 0.68-1.15 μm were observed for AY-TZP5-AY-TZP10 compared to those for AY-TZP.

The Vickers hardness (H_v) and fracture toughness (K_{1c}) of the different samples at 1300-1500 ^{o}C are presented in table 2. Similar H_v values were found for each composition at the different sintering temperatures. The maximum H_v values were found for AY-TZP, the addition of CaPSi glass gradually decreased the hardness. The K_{1c} values of AY-TZP and AY-TZP5- AY-TZP10 at 1300-1500 ^{o}C gave similar average results (4.2-4.8 MPa.m$^{1/2}$). The SEM observation of the induced crack propagation path after Vickers indentation revealed intergranular crack path in all the ceramics; thus, the crack propagated around ZrO_2 grains being deviated by them.

4. DISCUSSION

For 35 vol% slips, the NH_4PA concentration that gave minimum viscosity values increased from 0.88 wt% for AY-TZP to 1.26 wt% and 1.47 wt% for AY-TZP5 and AY-TZP10, respectively. Thus, the optimum NH_4PA concentration of AY-TZP5 and AY-TZP10 was found to be about 43 and 67 % greater than that of AY-TZP slips. Since the

negative zeta potential values of AY-TZP and CaPSi glass powder at pH 9 were similar (fig. 2), a significant variation of the negative zeta potential of AY-TZP5 and AY-TZP10 powders at that pH could not be expected. The greater NH_4PA adsorption with increasing CaPSi glass content could not be related to the zeta potential of the powders with different compositions, instead it could be explained considering the ionic strength of the suspensions.

The variation of pH with increasing solid concentration during the aqueous colloidal processing of 35 vol% slips (fig. 5), showed that the addition of AY-TZP5 and AY-TZP10 to the aqueous solution produced a greater increase in pH compared to that of AY-TZP. Thus, the substitution of AY-TZP by 5.4 and 10.5 vol% CaPSi glass increased the pH of the suspension. The increase in pH by the addition of AY-TZP5 and AY-TZP10 powders could be explained by the following ion exchange reaction at the CaPSi glass surface:

$$Si\text{-}O^- M^+ + H^+ + OH^- \rightarrow Si\text{-}OH + M^+ + OH^- \qquad (4)$$

The metal ion (M^+) is Ca^{2+} for CaPSi glass. Thus, an exchange reaction between H^+ and Ca^{2+} was involved in the uptake of H^+ by CaPSi glass surfaces. The uptake of H^+ and consequently the Ca^{2+} release via Ca^{2+}/ H^+ exchange reaction were expected to increase with increasing the amount of CaPSi glass. Thus, the increase in pH upon the addition of the powders to the aqueous solution was more pronounced with increasing CaPSi glass content. This glass dissolution behaviour was similar to those observed for many oxide ceramics containing cations in their crystal structure[26,27]. Sakar-Deliormanli et al[27] investigated the dissolution of Mg^{2+} and Pb^{2+} ions from lead magnesium niobate powder as a function of pH. They found that the amount of cations leached from the powder surface decreased as the pH increased. Our results showed that the dissolution of the CaPSi glass decreased with increasing solid concentration over 0.72 and 0.76 g/ml for AY-TZP5 and AY-TZP10, respectively, as a consequence of the increase in pH (Eq. 4 and fig. 5). Greater amounts of Ca^{2+} ions leached out from the CaPSi glass surface could be expected in AY-TZP5 and AY-TZP10 suspensions.

Guldberg-Petersen et al.[28] studied the effect of pH and ionic strength on the adsorption kinetics of polyacrylic acid on zirconia, and the resulting inter particle forces. Their results demonstrated that a relatively high ionic strength promoted a greater

polyelectrolyte adsorption. The polyelectrolyte adsorption is very sensitive to the level of ionic strength in suspensions[29]. Divalent cations can interact with two carboxylate ($^{-}$OOC-R) functional groups of the polyelectrolyte establishing counterion bindings; these ones can be either purely electrostatic or have an additional chemical interaction leading to cross-linking[30]. It has been reported[29-31] that divalent cations formed chemical complexes with acid polyacrylic (PAA). Bell et al[31] found that chemical complexes between PAA and barium ions were formed in the adsorbed polyacrylate layer. According to Bell[31], this behaviour was contrary to expectations for polyelectrolyte collapse resulting from purely electrostatic screening of polyelectrolyte charge sites. Vermohlen et al[32] investigated the effect of Ca^{2+} ions on the adsorption of acrylic based polyelectrolytes onto oxide surfaces. They reported that the plateau value of the adsorption isotherms was significantly increased by Ca^{2+} ions addition. Sakar-Deliormanli et al[29] studied the effect of $MgCl_2$ addition on the adsorption mechanism of PAA on lead magnesium niobate powders. They showed that the addition of Mg^{2+} ions increased the PAA adsorption nearly 2.6 times. This effect was directly related with the complex formation between PAA and Mg^{2+} ions. In the present study, the Ca^{2+} ions leached out from the CaPSi glass surface could form chemical complexes with NH_4PA, increasing the affinity of the polymer for the AY-TZP5 and AY-TZP10 surfaces and thereby the polymer adsorption. As a consequence, for 35 vol% slips the greater NH_4PA adsorption with increasing CaPSi glass could be attributed to the increasing amounts of Ca^{2+} ions in the suspensions.

A strong thixotropic behaviour was observed for flocculated 35 vol% slips (fig. 6), as the shear rate increased (up curve) the flocs were broken down by the hydrodynamic forces resulting in a decrease in the floc size. When the shear rate gradually decreased (down curve) lower viscosities were achieved due to a reduction in the characteristic floc size. For each slip composition, the degree of thixotropy notably decreased for well dispersed suspensions, reaching the minimum hysteresis loop area at the optimum NH_4PA concentration.

The rheological behaviour of stabilized 35 vol% slips did not significantly change by the addition of CaPSi glass (figs. 7a and 8), indicating that for this solid loading the different Ca^{2+} release of the suspensions did not greatly affect the colloidal stability of the slips. However, a different behaviour was found for 40 vol% slips, the viscosity and k attained minimum values at 5.4 vol% CaPSi glass. When the particles are forced together

by increasing the solid loading to 40 vol%, the separation between particles became shorter. In this case the inter particle forces were more sensitive to the ionic strength of the different suspensions. As it was previously mentioned, the electrostatic and steric components of the adsorbed polymer contributed to stabilize the suspensions. Bell et al[31] demonstrated that the presence of Ba^{2+} cross-linked PAA surface layers increased the resistance to compression of the polymer units, preventing collapse and maintaining a steric shell. Thus, the adsorbed polyelectrolyte layer was less likely to be compressed by the presence of divalent cations, resulting in polymer chains protruding into the solution. The formation of complexes in the adsorbed layer reduces the electrostatic charge of the polymer and consequently affects the electrostatic repulsive forces between the polyelectrolyte chains[30]. Therefore, complexation in adsorbed layers not only reduces the electrostatic component of the repulsive interaction, but also leads to thick steric layers[30].

As stated previously, the amount of NH_4PA adsorbed and consequently the thickness of the adsorbed layer increased with increasing CaPSi glass content, due to the greater amounts of Ca^{2+} leached out from the glass surface. The lower NH_4PA adsorption on stabilized AY-TZP slips, compared to that on AY-TZP5 and AY-TZP10 slips, could produce thinner adsorbed layers having higher net surface charge (fig. 4) and increasing the magnitude of the electrostatic interaction. On the other hand, the relatively higher Ca^{2+} release of stabilized AY-TZP10 slips could result in thicker adsorbed layers increasing the steric contribution, but decreasing the negative zeta potential of the NH_4PA adsorbed-powder (fig. 4). The minimum viscosity and k values of 40 vol% AY-TZP5 slips seemed to be an intermediate situation between a high electrostatic interaction (for AY-TZP slips) and a high steric interaction (for AY-TZP10 slips).

Clearly, the viscosity of the slips with different amounts of CaPSi glass was strongly influenced by the solid concentration. A comparison between the k values versus CaPSi glass content for 35 and 40 vol% slips (fig. 8), indicated that k significantly increased with the increase in the volume fraction of solids, as expected. At higher solid concentration, the resistance to flow increases because particles have to move out of each other's way, requiring higher stress values for flowing under shear[33].

The hysteresis loop area as a function of the CaPSi glass content for stabilized slips with different volume fraction of solids (figure 9), showed that the hysteresis area was reduced by the addition of 10.5 and 5.4 vol% CaPSi glass for 35 and 40 vol% slips,

respectively. In concentrated stabilized suspensions, i. e. non-aggregated slips, the velocity gradient imposes at high shear rates induces an orientation of the particle structure[33,34]. This orientation enables particles to move more freely than at low shear rates, leading to a decrease in viscosity. At even higher shear rates, the greater orientation of the particle structure produces particle layers separated by clear layers of liquid[34]. In this condition, the viscosity achieves its minimum value. The hysteresis behaviour observed cycling down in shear rate resulted in hysteresis loops. When shearing is reduced (down curve) the flow-induced layered structure gradually disappears. At low shear rates, the structure of the suspension is close to the equilibrium structure at rest because the Brownian forces dominates over the viscous forces[33,34].

The Brownian motion is characterized by a random disordered state in which particles are in constant movement. The Brownian force of the fine AY-TZP particles ensured that they were in movement. Some authors[33-35] related the thixotropic behaviour to the difference in the rates of dis-arrangement of the particles by shearing and that of arrangement when the stress is removed. The strong thixotropic behaviour of concentrated AY-TZP slips suggested that the break down of the structure under shear stress occurred at a higher rate than the rebuilding of the structure. The presence of CaPSi glass, with greater particle sizes relative to those of AY-TZP, could disturb the Brownian motion of the fine AY-TZP particles and induced the recovery of the structure when shear stress was removed. Therefore, the addition of CaPSi glass particles resulted in suspensions less prone to time-dependent effects. This behaviour occurred at 10.5 and 5.4 vol% CaPSi glass addition for 35 and 40 vol% slips, respectively. As the solid loading increased the average particle distance became shorter and lower amounts of CaPSi glass particles were able to disturb the AY-TZP particle movement.

The sintered density results indicated that the addition of 5.4 vol% CaPSi glass accelerated the densification of AY-TZP (table 2). AY-TZP5 can be sintered at a lower temperature (1300 ^{o}C) compared to that of AY-TZP by the densification acceleration effect of CaPSi glass. This finding was previously observed by us in the sintering of undoped-Y-TZP with CaPSi glass additive[6]. We have demonstrated that the addition of CaPSi glass increased the initial sintering rate through the decrease in the activation energy and the increase in the order of diffusion with respect to those previously reported for Y-TZP.

At 1300-1400 °C only t-ZrO_2 was present in AY-TZP; at 1500 °C a small amount of m-ZrO_2 appeared. The ZrO_2 grain size distribution of AY-TZP shifted to greater sizes with increasing sintering temperature; it should be noticed that the wide of the ZrO_2 grain size distribution increased gradually up to 1400 °C and then rapidly above this temperature. The XRD results (fig. 12) revealed that Y^{3+} along with Hf^{4+} ions migrated to grain boundaries at 1300-1400 °C. Sakka et al[36] also reported the cation diffusion to grain boundaries in Y_2 O_3 -$(Z_{r1-x}$ $Hf_x)O_2$ system. According to Cahn[37], the grain growth mechanism in Y-TZP is interpreted by the solute-drag effect of Y^{3+} ions segregating along grain boundaries. The segregation of Al^{3+} along with Hf^{4+} ions was found at 1500 °C; thus, Al^{3+} ions rather than Y^{3+} ions segregated at grain boundaries at 1500 °C. Similar results pertaining the Al^{3+} segregation behaviour in Al_2O_3-doped Y-TZP sintered at high temperatures have been reported by Matsui et al[38,39]. They explained that ZrO_2 grain growth was controlled by the segregated amount of Y^{3+} ions, however ZrO_2 grain growth was accelerated when the amount of segregated Al^{3+} ions exceeded a certain value. Yoshida et al[40] have studied the effect of small amounts of dopants on the ZrO_2 grain growth. They demonstrated that the grain boundary diffusivity increased as the ionic radius of dopant decreased. As the ionic radius of Al^{3+} ions (0.068 nm) is smaller than that of Y^{3+} ions (0.104 nm), in the present study the predominant effect that enhanced grain boundary diffusion and consequently ZrO_2 grain growth at 1500 °C (fig. 11) could be attributed to the segregated Al^{3+} ions rather than segregated Y^{3+} ions. The greater ZrO_2 grain growth in AY-TZP at 1500 °C let to a lesser stability of the t-ZrO_2 phase (table 3).

t-ZrO_2 was retained by the addition of CaPSi glass at 1300-1400 °C; on the contrary, at 1500 °C the addition of glass promoted the t-m ZrO_2 transformation (table 3). It has demonstrated (fig. 11) that the addition of CaPSi glass slightly shifted the ZrO_2 grain size distribution of AY-TZP to greater sizes at 1300-1400 °C; however at 1500 °C a markedly shifted to greater sizes by the addition of CaPSi glass was found. It has been previously found[6] that most of the SiO_2 produced by the glass decomposition formed $ZrSiO_4$ and a low amount of amorphous SiO_2 persisted in the compacts sintered at 1300-1500 °C. Ikuhara et al[41] investigated the solute segregation at grain boundaries in SiO_2-doped Y-TZP, they observed that Si^{4+} ions dissolved into tetragonal zirconia grains and segregated at grain boundaries, leading to grain boundaries migration and grain growth. In the present study, when Al^{3+} ions were mainly distributed in the ZrO_2 grain interior (low

segregation of Al^{3+}, fig. 12) at 1300-1400 ^oC, the dissolution of Si^{4+} ions into ZrO_2 grains seemed not to be favoured. In this case the SiO_2 -based amorphous phase did not significantly enhance the ZrO_2 grain growth (fig. 11). As the Al^{3+} segregation at grain boundaries became greater at 1500 ^oC (fig. 12), more Si^{4+} ions could dissolve and migrated to grain boundaries, promoting the ZrO_2 grain growth (fig. 11).

The increasing tendency in the ZrO_2 grain size with CaPSi glass additions at 1500 ^oC enhanced the t-m ZrO_2 transformation after sintering; while the lesser ZrO_2 grain growth by the presence of CaPSi glass at 1300-1400 ^oC retained the t- ZrO_2 phase upon sintering (fig. 11 and table 3). AY-TZP5 and AY-TZP10 at 1300-1400 ^oC were constituted by polygonal particles of $ZrSiO_4$ and elongated ones of $Ca_2P_2O_7$, uniformly distributed in the t-ZrO_2 fine grain matrix.

The decrease in the relative density of AY-TZP and AY-TZP5 at 1500 ^oC (table 2) could be explained considering the pronounced ZrO_2 grain growth which reduced the driving force for sintering.

The Vickers hardness had maximum values for AY-TZP, the addition of CaPSi glass gradually reduced the hardness. This behaviour could be explained taking into account that the hardness of Y-TZP (H_v ~13 GPa) was higher than those of $ZrSiO_4$ (H_v ~10-11 GPa) and calcium phosphate (H_v ~4-5 GPa), thereby the presence of these additional phases in the sintered ceramics reduced the H_v values.

AY-TZP5 and AY-TZP10 presented similar K_{1c} values with respect to that of AY-TZP. In all the samples, the ZrO_2 grains were not crossed by the crack tips, instead the induced crack propagated around ZrO_2 grains, therefore the t-m ZrO_2 transformation by a mechanical stress was not expected. Thus, the fracture energy absorption was related to crack deflection around ZrO_2 grains.

AY-TZP5 can be sintered at a lower temperature (1300 ^oC) compared to that of AY-TZP by the densification acceleration effect of CaPSi glass. AY-TZP5 at 1300 ^oC exhibited a fine microstructure of t- ZrO_2 (grain sizes below 0.3 μm), and $ZrSiO_4$ - $Ca_2P_2O_7$ particles homogeneously distributed within the ZrO_2 matrix. In comparison to AY-TZP, AY-TZP5 presented similar fracture toughness and a slightly lower hardness. The combined effects of the Al_2O_3-doping, the fine ZrO_2 grain sizes, and the present of additional phases, are expected to improve the ageing resistant of AY-TZP5 increasing the reliability of dental restorations based on zirconia. In a previous study[20], we have

determined that the presence of $Ca_2P_2O_7$ on undoped-Y-TZP surfaces promoted the osteogenic potential of UMR-106 cells. In vitro biological test as well as ageing experiments, will be conducted on AY-TZP5 surface to investigate its osteoblast cell response and ageing behaviour.

CONCLUSIONS

Well dispersed concentrated aqueous suspensions of Al_2O_3-doped Y-TZP (AY-TZP), AY-TZP with 5.4 vol% CaPSi glass (AY-TZP5) and 10.5 vol% CaPSi glass (AY-TZP10), with ammonium polyacrylate (NH_4PA) dispersant were prepared to produce slip cast compacts. The influence of CaPSi glass addition on the colloidal stability and rheological properties of 35 and 40 vol% AY-TZP slips was studied. The densification behaviour, microstructure as well as hardness and fracture toughness were investigated as a function of CaPSi glass content and sintering temperature. The optimum NH_4PA concentration of 35 vol% AY-TZP5 and AY-TZP10 slips at pH ~9 was found to be about 43 and 67 % greater than that of AY-TZP slips. The greater NH_4PA adsorption with increasing CaPSi glass content was related to the greater amounts of Ca^{2+} ions leached out from the CaPSi glass surface. The minimum viscosity of stabilized 40 vol% slips with NH_4PA occurred at 5.4 vol% CaPSi glass addition, and resulted in a more dense packing of cast samples.

AY-TZP5 can be sintered at a lower temperature (1300 ^oC) compared to that of AY-TZP by the densification acceleration effect of CaPSi glass. The increase in the ZrO_2 grain size with CaPSi glass additions at 1500 ^oC enhanced the t-m ZrO_2 transformation after sintering; while the lesser ZrO_2 grain growth by the presence of CaPSi glass at 1300-1400 ^oC resulted in the retention of t- ZrO_2 upon sintering. AY-TZP5 at 1300 ^oC exhibited a fine microstructure of t- ZrO_2 (grain sizes below 0.3 μm), and $ZrSiO_4$ - $Ca_2P_2O_7$ particles homogeneously distributed within the zirconia matrix. In comparison to AY-TZP, AY-TZP5 presented similar fracture toughness and a slightly lower hardness. The combined effects of the Al_2O_3 -doping, the fine ZrO_2 grains, and the present of additional phases, are expected to improve the AY-TZP5 ageing resistance increasing the reliability of dental restorations based on zirconia.

ACKNOWLEDGEMENT

This work was financially supported by CONICET (PIP 0454).

REFERENCES

1. Denry I, Kelly JR. State of the art of zirconia for dental applications. Dent. Mater. 2008;24:299-307.

2. Chevalier J. What future for zirconia as biomaterial?. Biomaterials 2006;27: 535-543.

3. Denry I, Kelly JR. Stabilized zirconia as a structural ceramic: an overview. Dent. Mater. 2008;24:289-298.

4. Ho WF, Hsu HC, Peng YF, Wu SC. Microstructure and mechanical properties of dental 3Y-TZP ceramics by using $CaO\text{-}P_2O_5$ glass as additive. Ceram. Int. 2011;37:1169-1174.

5. Santos C, Souza RC, Almeida N, Almeida FA, Silva RRF, Fernandes M H F V. Toughened ZrO_2 ceramics sintered with a La_2O_3-rich glass as additive. J. Mater. Process. Technol. 2008;200:126-132.

6. Stábile M F, Soubelet CG, Albano MP, Rosa AL, Moreira Spinola de Castro-Raucci L, Tambasco de Oliveira P. Effect of 64S bioglass addition on sintering kinetic, flexural strength and osteoblast cell response of Y-TZP ceramics. Int. J. Appl. Ceram. Technol. 2019;16: 517-530.

7. Piconi C, Maccauro G. Zirconia as a biomaterial, Biomaterials 1999;20:1-25.

8. Kohorst P, Borchers L, Strempel J, et al. Low-temperature degradation of different zirconia ceramics for dental applications. Acta Biomater. 2012;8:1213-1220.

9. Kosmac T, Kocjan A. Ageing of dental zirconia ceramics. J Eur Ceram Soc. 2012;32:2613-2622.

10. Li JF, Watanabe R. Influence of a small amount of Al_2O_3 addition on the transformation of Y_2O_3-partially stabilized ZrO_2 during annealing. J. Mater. Sci. 1997;32:1149-1153.

11. Wu Z-K, Li N, Jian CH, Zhao W-Q, Yan J-Z. Low temperature degradation of Al_2O_3 doped 3Y-TZP sintered at various temperatures. Ceram. Int. 2013;39:7199-7204.

12. Leo S, Tallon C, Stone N, Franks GV. Near-net-shaping methods for ceramic elements of (body) armor systems. J. Am. Ceram. Soc. 2014;97:3013-3033.

13. Olhero S, Ganesh I, Torres P, Alves F, Ferreira JMF. Aqueous colloidal processing of ZTA composites. J. Am. Ceram. Soc. 2009;92:9-16.

14. Ganesh I, Sundararajan G, Ferreira JMF. Aqueous slip casting and hydrolisis assisted solidification of $MgAl_2O_4$ spinel ceramics. Adv. Appl. Ceram. 2011;110:63-69.
15. Cesarano III J, Aksay IA. Processing of highly concentrated aqueous α-alumina suspensions stabilized with polyelectrolytes. J. Am. Ceram. Soc. 1988;71:1062-1067.
16. Hashiba M, Okamoto H, Nurishi Y, Hiramatsu K. Dispersion of ZrO_2 in aqueous suspensions by ammonium polyacrylate. J. Mater. Sci. 1989;24: 873-876.
17. Leong YK, Boger DV. Effect of polycarboxylate on the pH and magnitude of maximum yield stress of m-ZrO_2 suspensions. Ceramics Trans. 1991;19: 83-90.
18. Hench LL. The story of Bioglass. J. Mater. Sci. Mater. Med. 2006;17:967-978.
19. Jones JR. Review of bioactive glass: From Hench to hybrids. Acta Biomaterialia 2013;9:4457-4486.
20. Balamurugan A, Balossier G, Kannan S, Michel J, Rebelo AHS, Ferreira J M F. Development and in vitro characterization of sol-gel derived CaO-P_2O_5-SiO_2-ZnO bioglass. Acta Biomaterialia 2007;3:255-262.
21. Young RA. The Rietveld Method. International Un-ion Crystallography, Oxford University Press, Oxford, 1993.
22. Rodríguez-Carvajal J. Recent Developments of the Program FULLPROF, in Commission on Powder Diffraction (IUCr). Newsletter. 2001; 26:12-19.
23. Leong YK. Exploitation of interparticle forces in the processing of colloidal ceramic materials. Materials & Design 1994;15:141-147.
24. Mewis J, Wagner NJ. Thixotropy. Advances in Colloid and Interface Science 2009;147-148:214-227.
25. Benchabane A, Bekkour K. Rheological properties of carboxymethyl cellulose (CMC) solutions. Colloid Polym. Sci. 2008;286:1173-1180.
26. Paik U, Lee S, Hackley VA. Influence of barium dissolution on the electrokinetic properties of colloidal $BaTiO_3$ in an aqueous medium. J. Am. Ceram. Soc. 2003;86:1662-1668.
27. Sakar-Deliormanli A, Celik E, Polat M. Solubility and aging of lead magnesium niobate in water. Ceram. Int. 2009;35:503-508.
28. Guldberg-Pedersen H, Bergström L. Stabilizing ceramic suspensions using anionic polyelectrolytes: adsorption kinetics and interparticle forces. Acta Mater. 2000;48:4563-4570.

29. Sakar-Deliormanli A, Celik E, Polat M. Adsorption of anionic polyelectrolyte and comb polymers onto lead magnesium niobate. Colloids and Surfaces A: Physicochemical and Engineering Aspects 2008;316:202-209.
30. Bell NS, Monson TC, DiAntonio C, Wu Y. Practical colloidal processing of multication ceramics. J. Ceram. Sci. Tech. 2016;7:1-28.
31. Bell NS, Sindel J, Aldinger F, Sigmund WM. Cation-induced collapse of low-molecular-weigth polyacrylic acid in the dispersion of barium titanate. Journal of Colloid and Interface Science 2002;254:296-305.
32. Vermohlen K, Lewandowski H, Narres HD, Schwuger MJ. Adsorption of polyelectrolytes onto oxides-the influence of ionic strength, molar mass and Ca^{2+} ions. Colloids and Surfaces A: Physicochemical and Engineering Aspects 2000;163:45-53.
33.. Bergström L. Shear thinning and shear thickening of concentrated ceramic suspensions. Colloids and Surfaces A: Physicochemical and Engineering Aspects 1998;133:151-155.
34. Barnes HA. Shear thickening ("dilatancy") in suspensions of non aggregating solid particles dispersed in Newtonian liquids. J. Rheol. 1989;33: 329.
35. Ma J, Lin Y, Chen X, Zhao B, Zhang J. Flow behaviour, thixotropy and dynamical viscoelasticity of sodium alginate aqueous solutions. Food Hydrocolloids 2014;38:119-128.
36. Sakka Y, Oishi Y, Ando K. Zr-Hf interdiffusion in polycrystalline Y_2O_3-$(Zr+Hf)O_2$. J. Mater. Sci. 1982;17:3101-3105.
37. Cahn JW. The impurity-drag effect in grain boundary motion. Acta Metall. 1962;10:789-798.
38. Matsui K, Ohmichi N, Ohgai M, Yoshida H, Ikuhara Y. Effect of alumina-doping on grain boundary segregation-induced phase transformation in yttria-stabilized tetragonal zirconia polycrystal. J. Mater. Res. 2006;21:2278-2289.
39. Matsui K, Yoshida H, Ikuhara Y. Phase-transformation and grain-growth kinetics in yttria-stabilized tetragonal zirconia polycrystal doped with a small amount of alumina. J. Eur. Ceram. Soc. 2010;30:1679 -1690.
40. Yoshida H, Nagayama H, Sakuma T. Small dopant effect on static grain growth and flow stress in superplastic TZP. Mater. Trans. 2003;44:935 -939.

41. Ikuhara Y, Thavorniti P, Sakuma T. Solute segregation at grain boundaries in superplastic SiO_2-doped TZP Acta Mater. 1997;45:5275 -5284.

FIGURE CAPTIONS

Figure 1: Particle size distribution curves of AY-TZP and CaPSi glass powders.

Figure 2: Zeta potential versus pH curves of AY-TZP and CaPSi glass powders.

Figure 3: Flow curves of viscosity versus shear rate as a function of the amount of NH_4PA solution added at pH ~9 for different 35 vol% slips: (a) AY-TZP, (b) AY-TZP5, (c) AY-TZP10.

Figure 4: Zeta potential versus pH curves of different slips: AY-TZP with 0.88 wt% NH_4PA, AY-TZP5 with 1.26 wt% NH_4PA and AY-TZP10 with 1.47 wt% NH_4PA.

Figure 5: pH as a function of the solid concentration during the aqueous colloidal processing of 35 vol% AY-TZP, AY-TZP5 and AY-TZP10 suspensions.

Figure 6: Hysteresis loop area as a function of the NH_4PA concentration for the different 35 vol% slips.

Figure 7: Viscosity versus shear rate curves for 35 vol% (a) and 40 vol% (b) stabilized slips at pH ~9.

Figure 8: k rheological parameter, of the up flow curves, as a function of the CaPSi glass content for the different solid loading.

Figure 9: Hysteresis loop area as a function of the CaPSi glass content for stabilized slips with different volume fraction of solids.

Figure 10: SEM images of different sintered samples: (a) AY-TZP10 at 1300 ^oC, (b) AY-TZP5 at 1300 ^oC, (c) AY-TZP5 at 1400 ^oC.

Figure 11: ZrO_2 grain size distribution curves of different samples at 1300-1500 ^oC. Lines represent the normal curves fitted to experimental data.

Figure 12: XRD patterns of AY-TZP at 1300-1500 ^oC in the 2θ range of 26.5-27.7^o .

Table 1: Power-law model fitting parameters, k and n, of the up flow curves for 35 vol% AY-TZP, AY-TZP5 and AY-TZP10 slips as a function of the NH_4PA concentration.

Slip composition	NH_4PA concentration (wt%)	Power-law model fitting parameters		
		K ($Pa.s^n$)	n	R^2
AY-TZP	0.51	6.3014	0.3101	0.9967
	0.63	4.2026	0.3362	0.9951
	0.88	3.0353	0.3615	0.9929
	1.02	5.0385	0.3126	0.9949
AY-TZP5	1.07	15.6718	0.2517	0.9859
	1.16	12.0763	0.2803	0.9960
	1.26	3.4155	0.3415	0.9976
	1.35	6.0481	0.3112	0.9967
AY-TZP10	1.18	9,0188	0.2520	0.9927
	1.38	3.5104	0.3213	0.9943
	1.47	3.2282	0.3421	0.9891

Table 2: Relative density and mechanical properties of different samples sintered at 1300-1500 ^{o}C

Sample	Temperature (^{o}C)	Relative density (%)	Hardness (GPa)	Fracture toughness (MPa.m$^{1/2}$)
AY-TZP	1300	95.7	12.9 ± 0.1	4.5± 0.2
	1400	99.6	13.0 ± 0.2	4.7± 0.1
	1500	95.3	12.7 ± 0.3	4.3± 0.3
AY-TZP5	1300	99.7	11.8 ± 0.2	4.8± 0.2
	1400	99.6	11.9 ± 0.1	4.7± 0.4
	1500	95.2	11.6 ± 0.3	4.5± 0.1
AY-TZP10	1300	94.3	10.5 ± 0.1	4.2± 0.3
	1400	94.9	10.6 ± 0.2	4.3± 0.2

Table 3: Crystalline phase contents of different samples sintered at 1300-1500 ^{0}C.

Temperature (^{o}C)	AY-TZP		AY-TZP5				AY-TZP10			
	t- ZrO_2 content (vol%)	m- ZrO_2 content (vol%)	t- ZrO_2 content (vol%)	m- ZrO_2 content (vol%)	$Ca_2P_2O_7$ content (vol%)	$ZrSiO_4$ content (vol%)	t- ZrO_2 content (vol%)	m- ZrO_2 content (vol%)	$Ca_2P_2O_7$ content (vol%)	$ZrSiO_4$ content (vol%)
1300	100	0	95.4	0	1.5	3.1	91.7	0	2.8	5.5
1400	100	0	95.5	0	1.6	2.9	91.6	0	3.0	5.4
1500	98.8	1.2	88.3	7.2	1.7	2.8	82.1	9.4	2.9	5.6

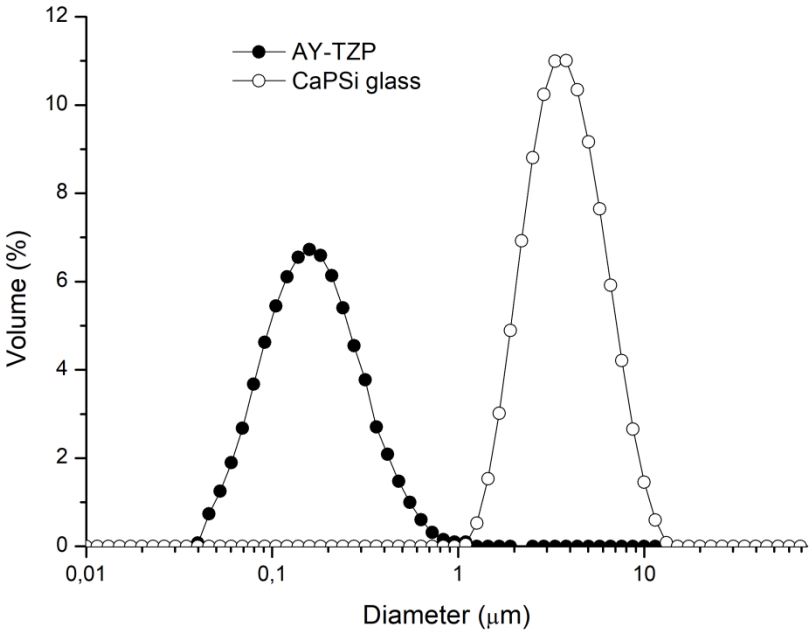

ijac_13420_f1.tif

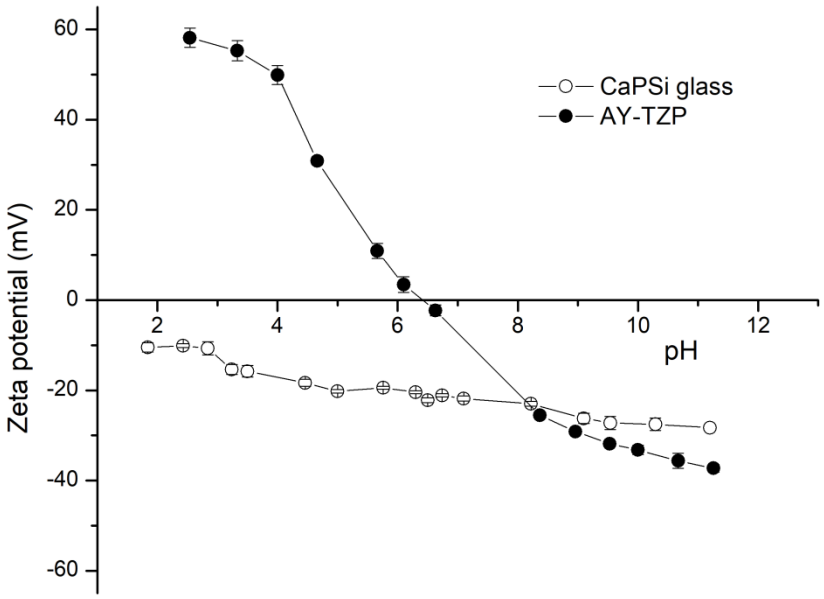

ijac_13420_f2.tif

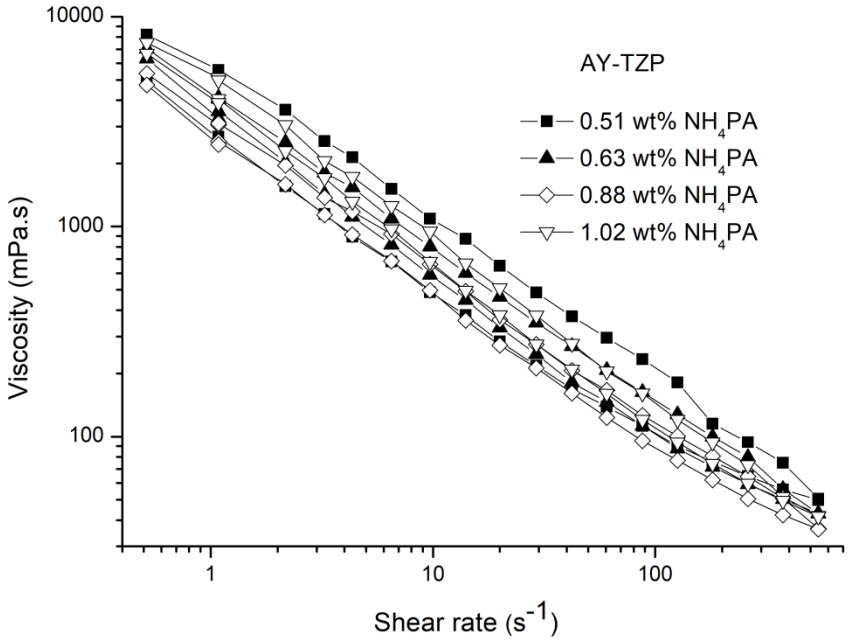

ijac_13420_f3a.tif

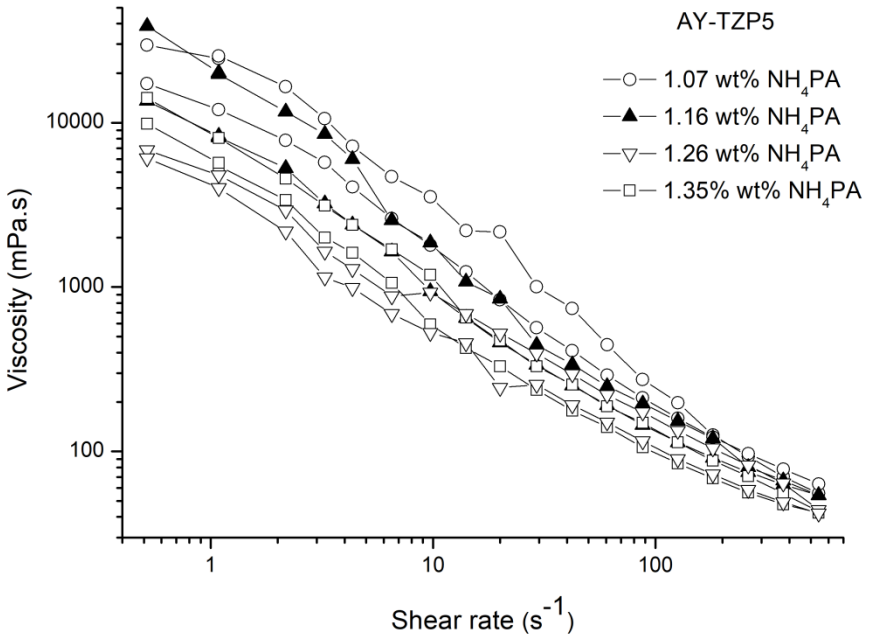

ijac_13420_f3b.tif

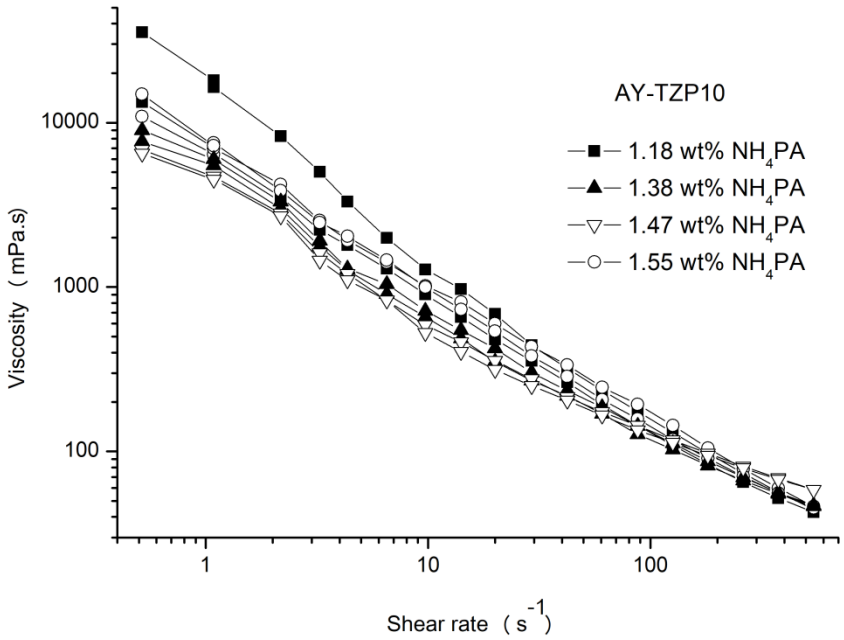

ijac_13420_f3c.tif

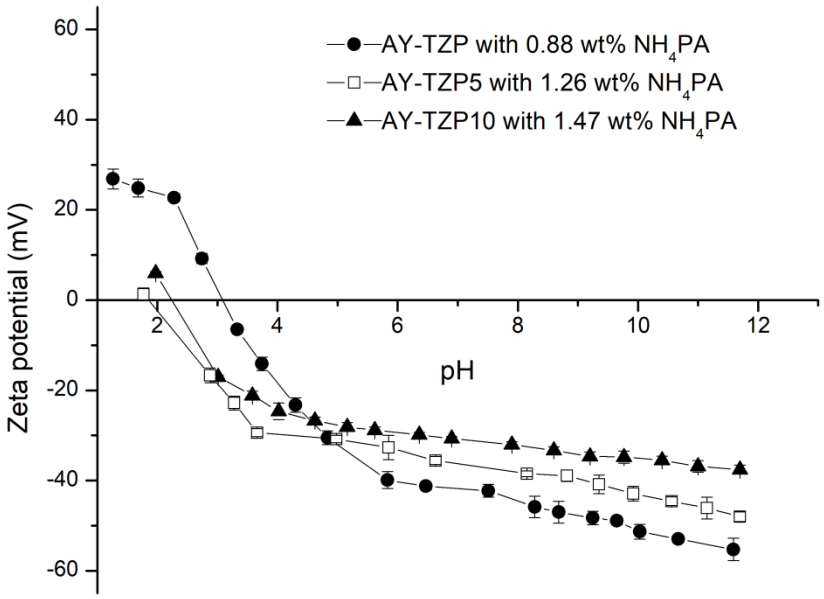

ijac_13420_f4.tif

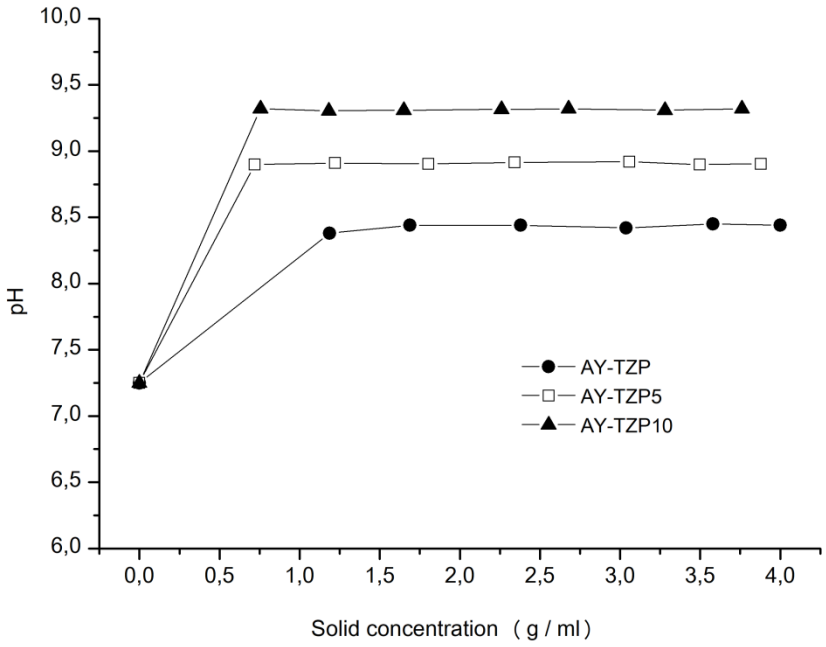

ijac_13420_f5.tif

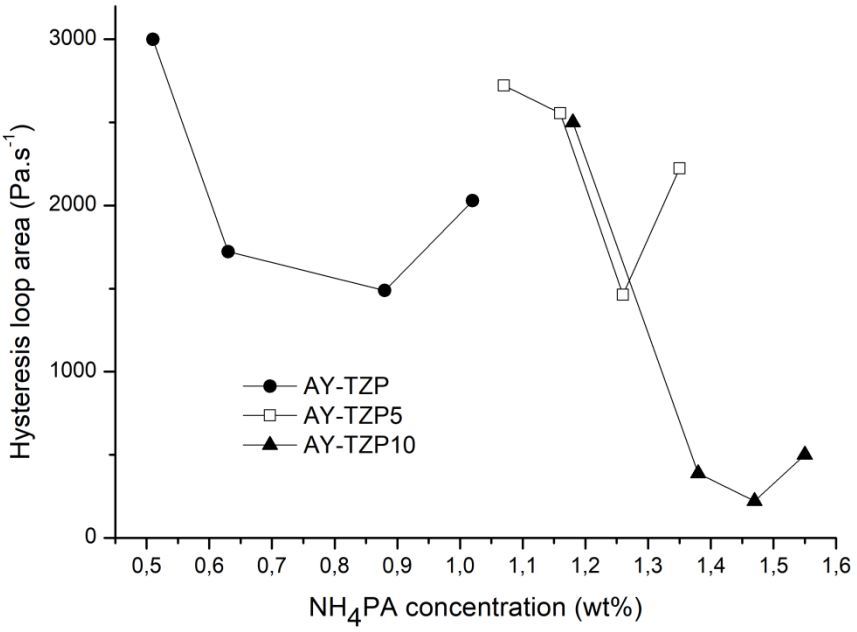

ijac_13420_f6.tif

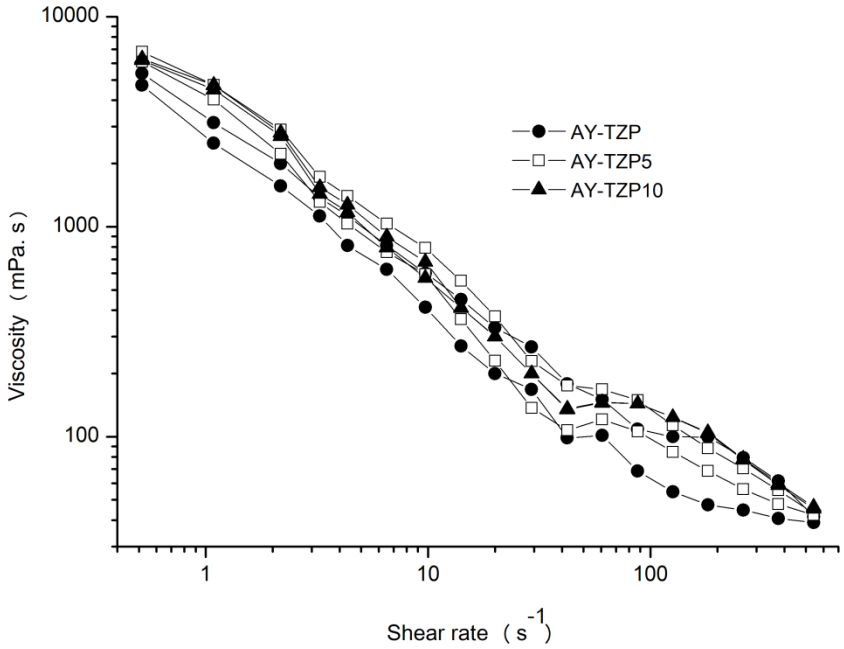

ijac_13420_f7a.tif

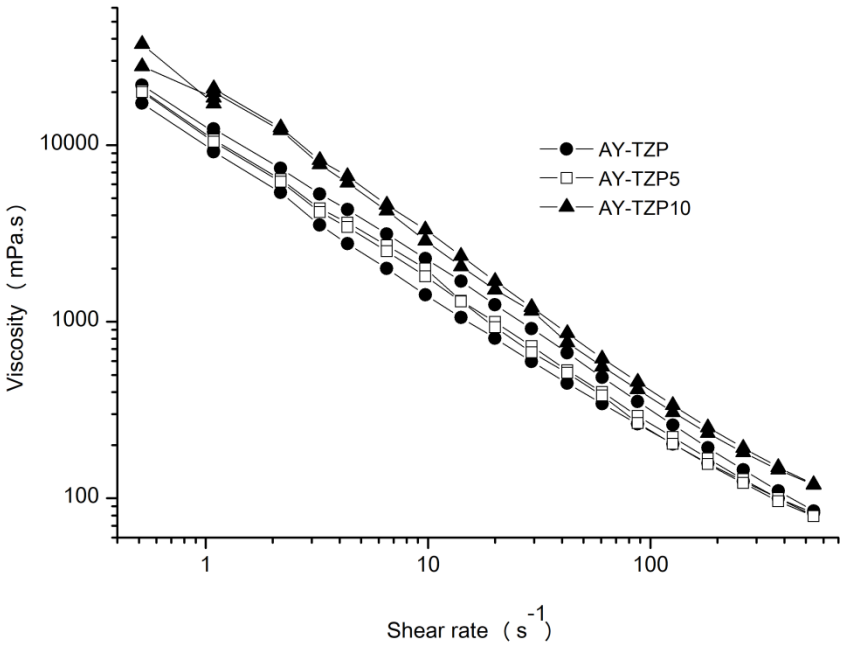

ijac_13420_f7b.tif

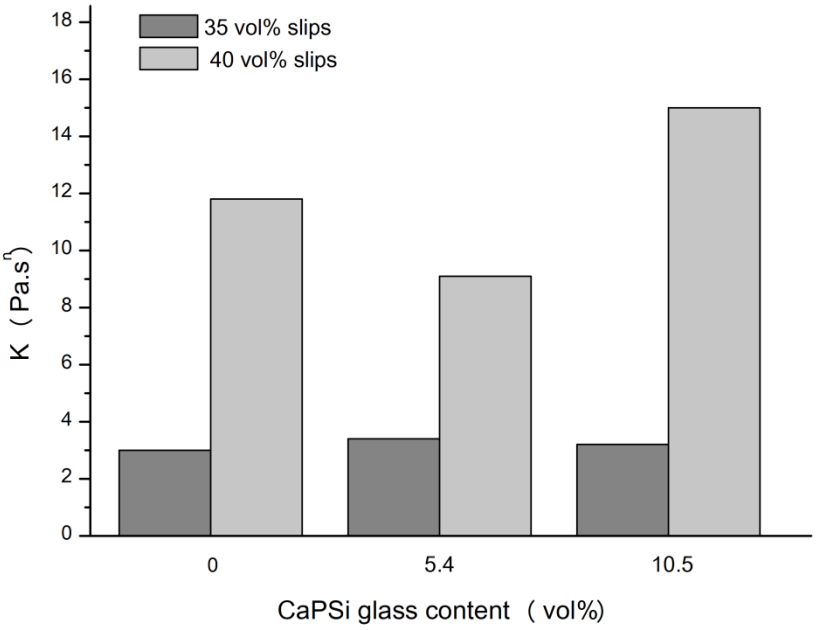

ijac_13420_f8.tif

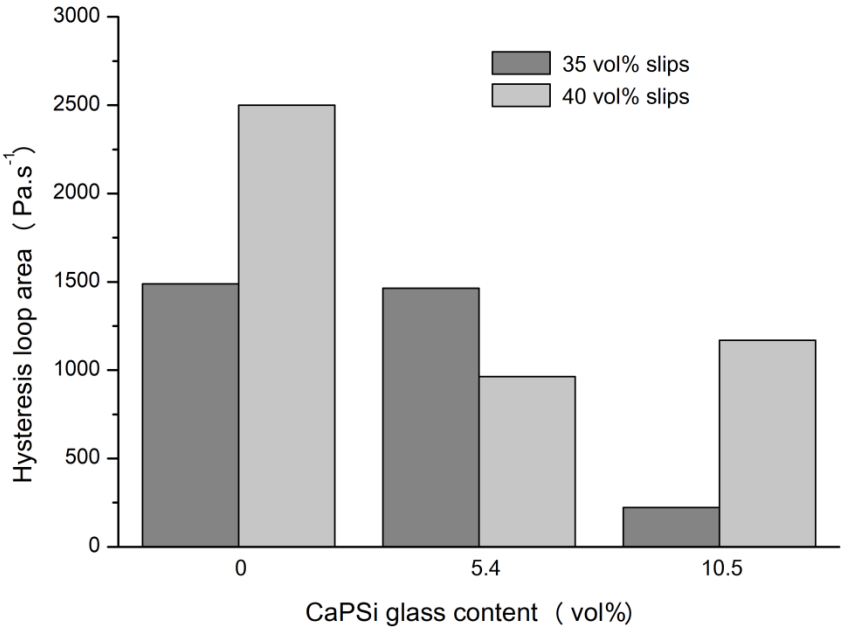

ijac_13420_f9.tif

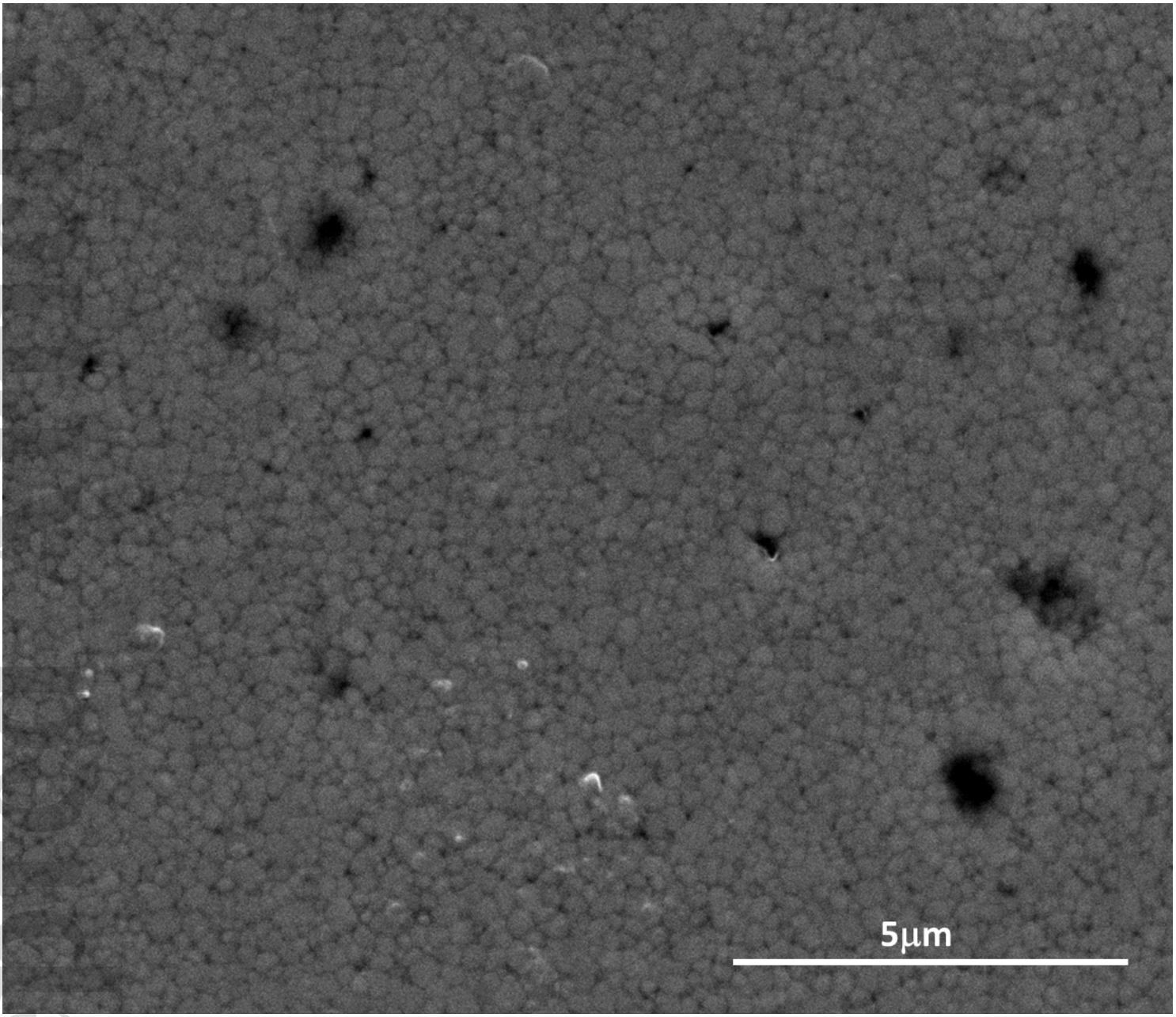

ijac_13420_f10a.tif

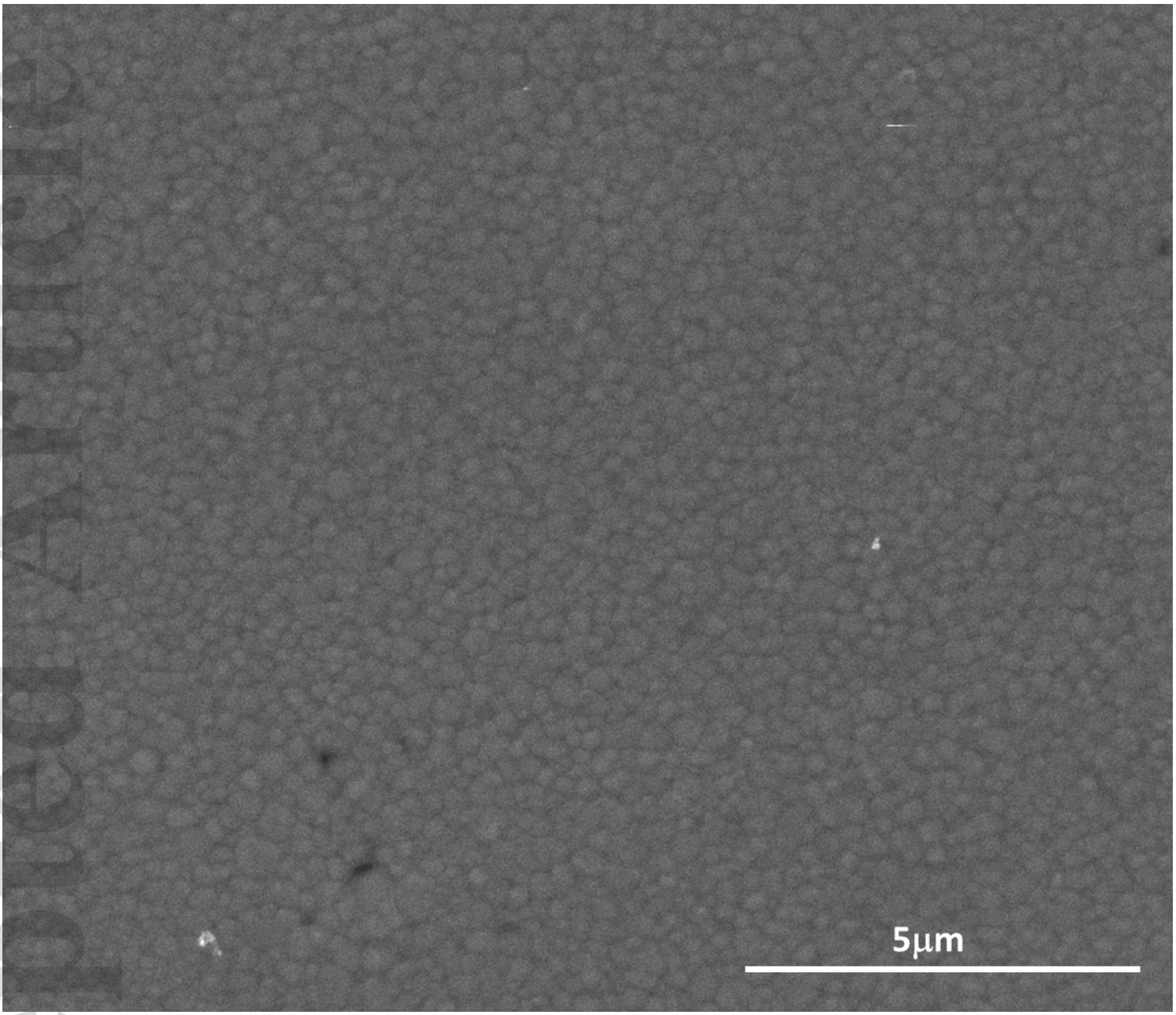

ijac_13420_f10b.tif

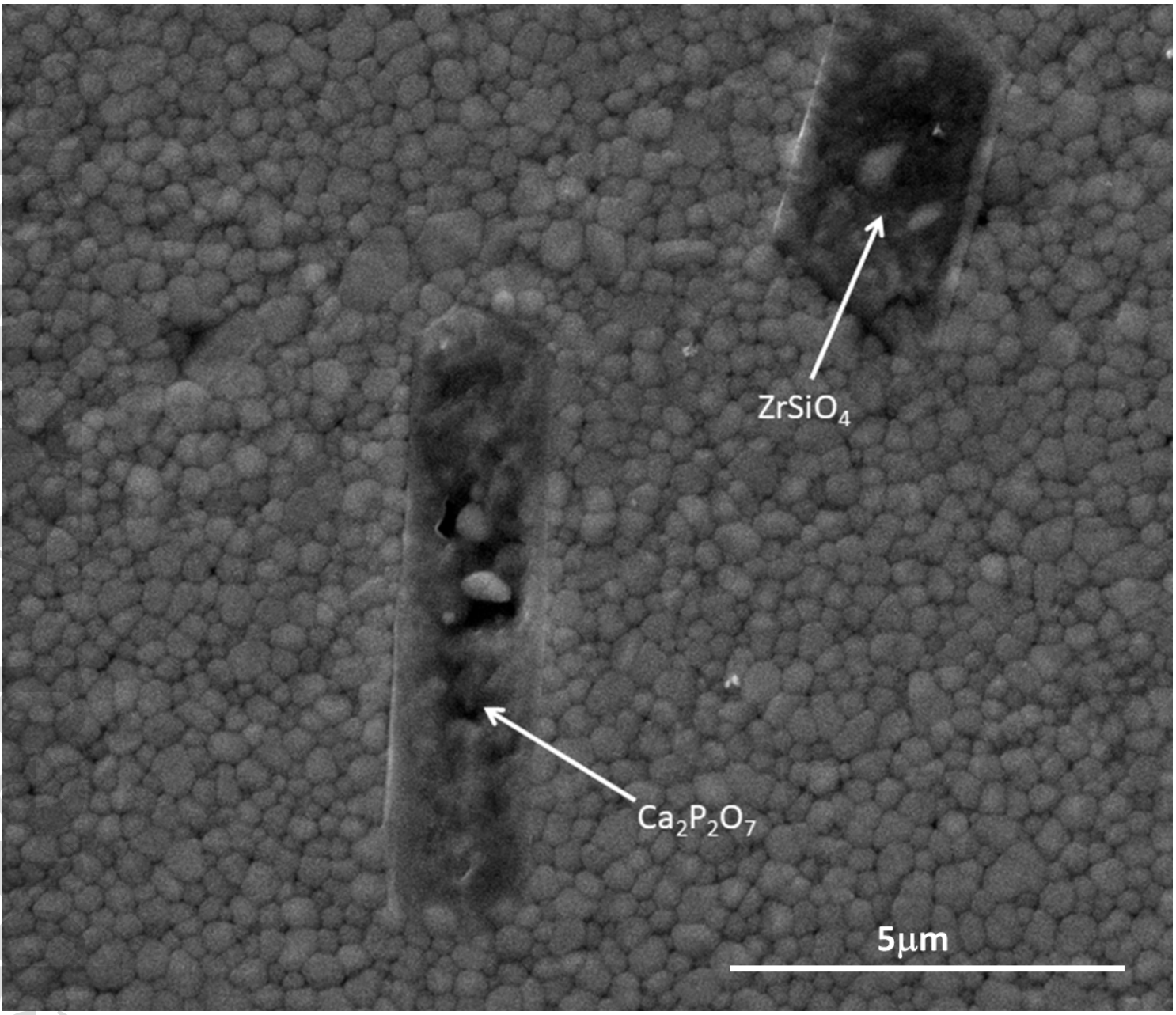

ijac_13420_f10c.tif

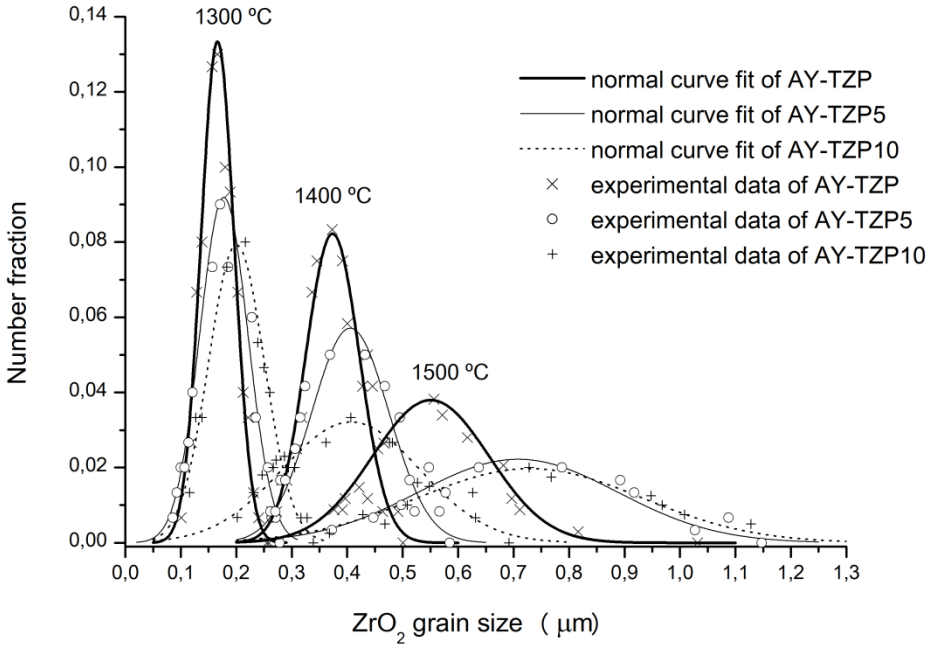

ijac_13420_f11.tif

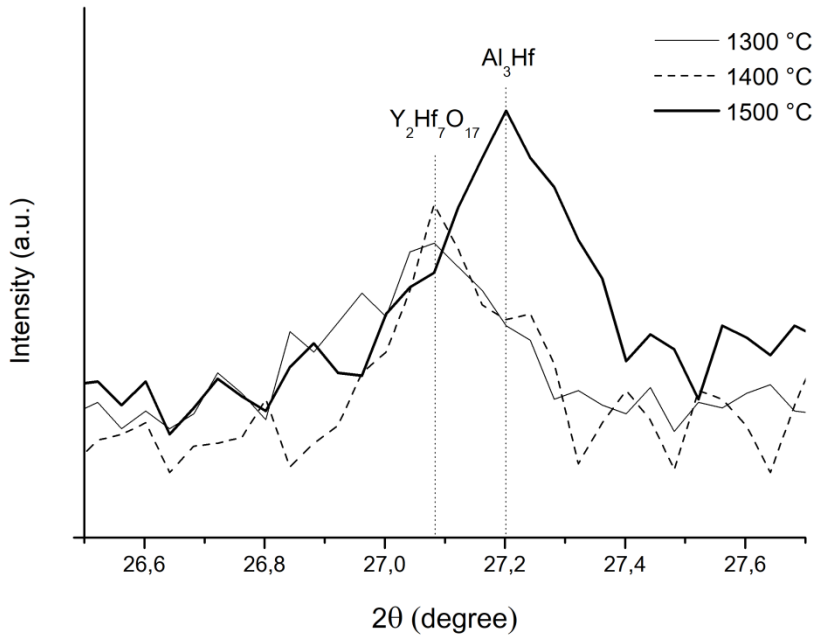

ijac_13420_f12.tif